Desalination and Water Treatment
www.deswater.com
doi: 10.1080/19443994.2015.1042067

57 (2016) 10959–10968
May

Taylor & Francis
Taylor & Francis Group

Microfiltration of cutting-oil emulsions enhanced by electrocoagulation

Janja Križan Milić[b], Emil Dražević[a,*], Krešimir Košutić[a], Marjana Simonič[b]

[a]*Faculty of Chemical Engineering and Technology, Department of Physical Chemistry, University of Zagreb, Marulićev trg 19, HR-10000 Zagreb, Croatia, Tel. +385 1 459 7240; emails: edraz@fkit.hr (E. Dražević), kkosutic@fkit.hr (K. Košutić)*
[b]*Faculty of Chemistry and Chemical Engineering, Laboratory for Water Treatment, University of Maribor, Smetanova 17, SI-2000 Maribor, Slovenia, emails: krizan.janja@gmail.com (J.K. Milić), marjana.simonic@um.si (M. Simonič)*

Received 17 November 2014; Accepted 10 April 2015

ABSTRACT

Electrocoagulation (EC) was examined as a pre-treatment to the microfiltration (MF) of oily emulsions within the metalworking industry. The aim of this pre-treatment was to improve the MF performance in terms of flux decline and removal of oil by applying the minimum time of EC pre-treatment. Aluminium electrodes were used in EC, and flat sheet-regenerated cellulose membrane in MF. The experiments were carried out using cutting-oil emulsions at different concentrations (0.1, 0.5 and 1.0% (v/v)) and conductivity of about 700 μS cm^{-1}. Drop size and zeta potential distributions were carried out to evaluate the impacts of EC time on zeta potential and average particle size. We found that in all emulsions, 10 min of EC made the average size of oil particles bigger than the average size of the pores in MF and substantially reduced pore clogging and irreversible fouling. Reduced flux decline was related to the continuous formation of $Al(OH)_3$ in EC that interconnected the colloidal oil particles into porous and irregularly shaped flocs which formed highly porous cake layer on the membrane surface.

Keywords: Microfiltration; Electrocoagulation (EC); Cutting-oil emulsion; Cake layer; Flux decline; Zeta potential

1. Introduction

Cutting-oil emulsions are used as lubricants and coolants specifically designed for metalworking processes. Used cutting-oils may cause high levels of contamination and rancid odours due to the presence of emulsifiers, corrosion inhibitors, extreme pressure agents, biocides or antifoam compounds. Their treatment and final disposal should be handled carefully [1].

Micro- and ultra-filtration (MF/UF) have arisen over time as an effective technology in the treatment of oily wastewaters as it offers high removal of oil, low-energy consumption and a compact design compared to robust space-consuming traditional processes [2–4]. The efficiency of MF/UF, however, may vary when considering fouling (e.g. pore-clogging) [5–9], flux decline and consequently change in rejection [6]. High water flux in MF/UF, along with high separation of oil and considerably low mass transfer of very big and slow diffusing oil molecules, causes 10-fold higher concentration of oil at the membrane surface [10,11]. Enhanced concentration of oil near the membrane surface may facilitate oil adsorption, and oil droplets may enter the membrane pores, i.e. clog them. In this way, irreversible fouling occurs [8,9,12]. Periodical hydraulic cleaning, such as backwashing, back-pulsing and

*Corresponding author.

1944-3994/1944-3986 © 2015 Balaban Desalination Publications. All rights reserved.

pulsing by filtration, can reduce irreversible fouling i.e. concentration polarisation or cake layer formation, while irreversible fouling caused by oil adsorption and pore plugging cannot be completely avoided without further chemical cleaning [4]. Chemical cleaning of a membrane to reduce or eliminate irreversible fouling should be limited to a minimum frequency because repeated chemical cleaning increase the cost of the MF process.

In practice, MF is always paired with a pre-treatment process [13,14], usually coagulation [15], which increases the size of the colloidal particles and prevents the irreversible fouling/flux decline [4]. The benefits of conventional coagulation coupled with membrane processes have been reported by many authors. For instance, several authors have reported that coagulation enabled the formation of a porous cake layer of flocs and reduced membrane fouling [5]. The porosity of a cake layer depends on the flocs' characteristics, such as irregularity and size, and the flocs' stabilities within a rectangular channel with a feed spacer that are affected by cross-flow-induced shear stress [5]. Conventional mineral coagulants such as Fe^{3+} may in some cases decrease fouling resistance of the membrane [16,17]. In addition, Al^{3+} and Fe^{3+} form less stable flocs that can be easily broken at the membrane's surface [5]. The polyelectrolytes used as coagulants form shear stress-resistant flocs; however, polyelectrolytes could potentially adsorb on the polymeric membrane surface and induce severe fouling [5]. Al^{3+} was found to be a fair coagulant [15], especially if the same amount was in two steps [13]. During the second step, $Al(OH)_{3(s)}$ precipitate was formed which enabled the formation of irregular flocs which later on formed porous cake layer on the membrane surface.

Electrocoagulation would appear as fairly good pre-treatment to filtration of cutting-oils [18–20], as compared to the conventional dosing of Al^{3+}, under the influence of an electric current, electrocoagulation produces metallic ions (Al^{3+}) *in situ*, by the electrochemical dissolution of electrode (anode). Dissolution of aluminium is always paired with the instant formation of OH^- and an increase in pH, resulting with the continuous formation of $Al(OH)_{3(s)}$. It has been suggested by some authors that EC should be used as a pre-treatment to MF, as it generates coagulants *in situ*, and thus reduces the chemical coagulant requirements [18,21] as well as it offers shorter coagulation times (faster particle growth) of irregularly formed flocs [22,23]. In other words, there is no need for two stage —conventional coagulation as $Al(OH)_{3(s)}$ precipitate is continuously formed *in situ* [24]. In addition, electrocoagulation may act beneficially in other ways and reduce the concentration of heavy metals and the chemical oxygen demand of the feed [25].

The main drawback of MF of cutting-oils is the flux reduction which is usually caused by the cake layer resistance. One of the ways to decrease the cake layer resistance is to increase the water permeability of the cake layer. Water permeability of the cake layer increases when the cake layer is formed of irregularly shaped flocs. The novelty of this study is in investigation of electrocoagulation as a pre-treatment to the MF of the cutting-oil emulsions. More detailed, the impacts of EC time on zeta potential and average particle size of cutting-oil emulsions on the efficiency of microfiltration were evaluated. Model cutting-oil emulsions and membrane were characterised using experimentally obtained drop size distribution and zeta potential (ζ) of a model emulsion and scanning electron microscope (SEM).

2. Materials and methods

2.1. Cutting-oil emulsion

The model cutting-oil emulsion was prepared by mixing commercial cutting-oil (Die-Lubric 7050) and deionised water. Commercial cutting-oil concentrate is, as its major part, made of polysiloxane. Its physical properties are; white colour, pH 9.5, density of 0.994 g mL^{-1} and dynamic viscosity of 0.0018 Pa s. The volume percentages of model cutting-oil emulsions in water were 0.1, 0.5 and 1% (v/v). The pH values of the model cutting-oil emulsions were between 6 and 7.5, depending on concentration. The conductivity of the emulsions was around 700 μS/cm.

2.2. Membrane characterisation: swelling, SEM and zeta potential measurements

A flat sheet polymeric (regenerated cellulose (RC) —UC030) membrane was kindly supplied by MICRODYN-NADIR GmbH (Wiesbaden, Germany). UC030 was selected due to its high water flux and good fouling resistance to organics [4].

Membrane swelling, i.e. water content of the RC membrane was determined in two ways;

(1) three-dimensional (3D) measurements of heights (d_z), widths (d_y) and lengths (d_x) of dry and wet samples, using precise digital calliper (Neiko 01407A) with an accuracy of ±0.01 mm, and
(2) from the difference in mass (m) of the dry and wet membrane samples. The readability of used digital analytical balance (KERN ALS 220-4, Balingen, Germany) was 0.0001 g with accuracy of ±0.0001 g.

Briefly, the measurements were performed as follows;

(1) measuring of height, weight, length and the mass of dry membrane samples (5×5 mm^2),
(2) wetting the dry membrane samples in deionised water for two hours, and
(3) removal of the excess deionised water with a dry paper towel and the repetition of step (1) for wet membrane samples.

$$\Phi = \frac{m_{\text{wet}} - m_{\text{dry}}}{m_{\text{wet}}} \quad (1)$$

The average swelling, Φ, is calculated using Eq. (5). The swelling in each of the three dimensions was estimated using the expression found below.

$$\Phi_{x,y \text{ or } z} = \frac{d_{x,y \text{ or } z \text{ wet}} - d_{x,y \text{ or } z \text{ dry}}}{d_{x,y \text{ or } z \text{ wet}}} 100 \quad (2)$$

A SEM (VEGA 3 SEM, TESCAN, a.s., Czech Republic) was used to estimate the pore size of the RC membrane. SEM images were recorded at 10 random 50×50 μm^2-sized surfaces of five different samples of RC membrane. Each of the five samples was taped to a stainless steel stub by carbon tape and placed into an ion sputter within an atmosphere of argon, where a thin layer of gold was deposited on each membrane's surface at 18 mA for 60 s. The samples were imaged at 5 kV at a working distance of about 5 mm and beam intensity of 10, thus achieving magnifications of up to 18,000 times. The above-described conditions allowed the measuring of pore sizes up to 5,000 nm, which was of practical use for the examined RC MF membrane. The pores' sizes were measured using VEGA built-in software.

The streaming current measurements were done using an electrokinetic analyser (SurPASS, Anton Paar GmbH, Austria) equipped with a cylindrical cell, where pieces of membrane ($2r > 25$ μm) were mounted into the measuring cell. The standard 0.001 mol L^{-1} solution of KCl was used as electrolyte in our experiments. Before each measurement, sample was rinsed with 0.001 mol L^{-1} solution of KCl. The zeta potential dependence on pH was studied within the range pH 3–10. pH was changed by adding drops of mol L^{-1} HCl or 0.1 mol L^{-1} NaOH. The zeta potential (ζ) was calculated from the measured streaming potential using the Fairbrother–Mastin equation, which takes into account any surface conductivity [2].

2.3. Electrocoagulation

Electrocoagulation was performed within a cylindrical batch reactor with 1 L of model emulsion using aluminium electrodes. The active surfaces of two electrodes were 4×5 cm^2 whilst the distance between the electrodes was fixed at 1 cm. The electrical current was maintained at a constant value $I = 200$ mA, which was found optimal current regarding the conductivity of the emulsions. The model emulsion was stirred during the experiment using a mechanical stirrer with a constant rotational speed of 200 rpm. The model emulsion's thermostat was at 25.0 ± 0.1℃ during all 30 min of the EC (Fig. 1). The electrodes were cleaned after every EC experiment using wet "Si–C" paper until the surface appeared smooth, in order to reduce passivation and remove oil deposition [26]. The oil layer induced by flotation remained non-skimmed and the *whole* model cutting-oil emulsion was moved to MF and filtered after 5, 10, 15 and 30 min of EC.

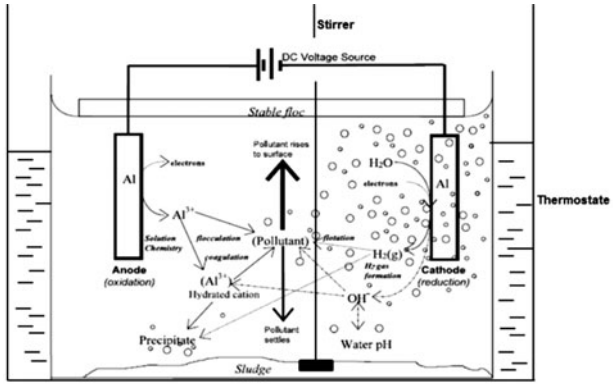

Fig. 1. Schematic representation of electrocoagulation [34].

2.4. Microfiltration

Microfiltration experiments were performed within a cross-flow Sepa CF II cell (Sterlitech Corporation, USA) of a membrane area of 0.0138 m^2 and channel dimensions of $14.5 \times 9.5 \times 0.17$ cm^3 (length × width × height). A feed spacer was used to improve the hydrodynamics in the channel. The feed from a 5 L tank was circulated through the cell at a flow rate of 3 L/min (cross-flow velocity 0.32 m/s) by means of a Hydracell DO3SASGSSSCA pump driven by a variable-speed motor (Wanner Engineering Inc., Minneapolis, USA). This cross-flow velocity was found optimal as it gives minimal concentration polarisation at minimum pressure drop. All microfiltration experiments were carried out at a constant temperature of 25.0 ± 0.1℃, using a thermostat and a Danfoss XG10 heat exchanger.

At the beginning of each experiment, the flux was stabilised at 2 bar for 3 h with DI water until a steady

state was reached. The pressure during all the experiments was set at 1 bar. Firstly, the initial DI water flux J_{wi}, L/(m^2 h^{-1}) was measured by collecting and measuring the permeate volume over a certain time and dividing it by a nominal membrane surface. Then the tank was emptied, refilled with cutting-oil emulsion and the permeate flux $J_{s,}$ L m^{-2} h^{-1} was measured. After 2 h of microfiltration, the membranes were flushed with DI water for 20 min, and then the water flux, J_{wc}, L m^{-2} h^{-1}was measured. Virgin RC membrane was used during each experiment.

The concentrations of oil in both the permeate and retentate streams of MF were analysed using a carbon analyser (TOC-V$_{WS}$ Shimadzu, Japan) in three replicates. Removal of oil from the wastewater, R, %, was calculated on the basis of total carbon concentration, as described below.

$$R = \left(1 - \frac{C_p}{C_f}\right)100 \tag{3}$$

In Eq. (3), C_f is the concentration of oil in the retentate stream, mg L^{-1}, and C_p the concentration of the oil in the permeated stream, mg L^{-1}.

Flux decline occurred as a result of two different phenomena; concentration polarisation, i.e. resistance of the cake layer, and oil adsorption/pore plugging [8]. Therefore, it was quantified by correlating it to specific phenomena, as described below [8,27]:

$$\mathrm{FR} = \frac{J_{wi} - J_s}{J_{wi}}100 \tag{4}$$

In Eq. (4), the FR %, is the total flux decline caused by concentration polarisation, cake layer resistance and membrane fouling, J_{wi} is the initial virgin membrane flux measured with pure deionised water and J_s is the permeate flux measured with model cutting-oil emulsion.

$$\mathrm{FR_{ADS}} = \frac{J_{wi} - J_{wc}}{J_{wi}}100 \tag{5}$$

In Eq. (5), the FR$_{ADS}$ % is the flux decline caused by oil adsorption and pore plugging, and J_{wc} is the water flux measured with DI after membrane was being flushed with DI.

$$\mathrm{FR_{CP}} = \mathrm{FR} - \mathrm{FR_{ADS}} \tag{6}$$

In Eq. (6), the FR$_{CP}$ % is the flux decline caused by concentration polarisation and cake layer formation.

2.5 Particle size measurements

The particle size/oil droplets size distributions and zeta potentials (in liquid emulsion) measurements were performed using the Zetasizer Nano ZS instrument (Malvern Instruments, UK) equipped with dynamic light scattering and laser Doppler micro-electrophoresis. Zeta potential measurements of the model cutting-oil emulsions, 0.1, 0.5 and 1% (v/v), were carried out after 5, 10, 15 and 30 min of EC in order to obtain zeta potential vs. time of EC curves.

3. Results and discussion

3.1. Membrane characterisation

Fig. 2(A) and (B) show that the UC030 membrane has bimodal pore size distribution with two average pore size radii, the smaller located roughly around 100 nm and bigger at about 1.5 μm. It was reported earlier by Persson et al. that even some UF membranes had bimodal pore size distributions [28]. Both of the average pore radii can thus play a substantial role in transport of oil droplets over the UC030 MF membrane. For instance, even if the sizes of the oil particles/droplets largely exceeded the smaller pores sizes, one could still expect a significant oil flux through the membrane. Fig. 2(B) shows that UC030 membrane had very high porosity which, along with bigger pores (voids), explained the extremely high water fluxes achieved by this membrane. It should be emphasized, however, that SEM provided information only on surface porosity and this membrane had asymmetric structure. For this reason, we estimated the average pore radii from water permeability and water content measurements, as explained below.

The water content of regenerated cellulose is presented in Table 1. It significantly swelled in water and

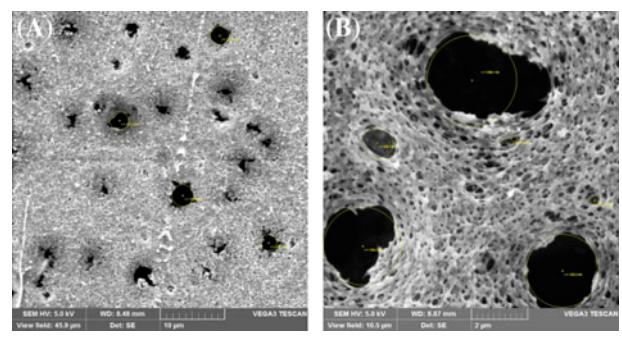

Fig. 2. SEM image of MF membrane; (A) An example of 50 × 50 μm^2 surface of MF UC030 membrane, working distance 8.48 mm, 5 kV. (B) 10 × 10 μm^2, closer look at smaller pores, working distance 8.87 mm, 5 kV.

Table 1
Three-dimensional (3D), Φ_x, Φ_y and Φ_z, and the average swelling of the RC membrane

3D swelling							
Φ_{xyz} (%)	errΦ_{xyz} (%)	Φ_x (%)	errΦ_x (%)	Φ_y (%)	errΦ_y (%)	Φ_z (%)	errΦ_z (%)
24.93	10.35	3.67	1.43	1.42	0.51	19.84	8.40
Swelling measured by mass							
Φ		errΦ					
0.3459		0.0065					

it three dimensionally shrank (Table 1) 20% in height, 1% in width and 4% in length. During the production and phase inversion of RC [31], a fast evaporation of the solvent might have occurred expanding the membrane structure in the x, y and z directions that after being equilibrated in water collapsed and shrank.

Average pore radius in the wet state was estimated from pure water permeability using the relationship proposed below [29].

$$L_p d_{z\text{wet}} = \frac{b r_p^2 \Phi}{\eta \alpha} \tag{7}$$

In Eq. (7), L_p, m Pa^{-1} s^{-1} is the pure water permeability, r_p, m is the pore radius, η, Pa s dynamic viscosity of the water, $d_{z\ \text{wet}}$, m is the measured swollen thickness of the membrane, Φ is the water content assumed to be equal to porosity and α tortuosity. Tortuosity may be estimated using its dependence on porosity (water content) given by Torquato [30]. Parameter b is a geometric parameter that depends on the pore geometry, and Torquato [30] suggests $b = 1/8$ for random porous media. An average hydraulic pore radius calculated using Eq. (7) was 82 nm, and is in fairly close agreement with Fig. 2, along with some other studies which examined membranes made of regenerated cellulose [31,32].

Fig. 3 shows the variation of the MF membrane zeta potential with the pH. It is noticed that UC030 membrane is negatively charged even at very low pH, which is unlikely to be the property of the pure regenerated cellulose. Even though manufacturer declared that UC030 membrane tested was made of regenerated cellulose (cellulose II), it is likely that they used the chemical post-treatment of RC that added acidic functional groups which now act as proton donor groups. The negative charge of MF membrane, i.e. dissociation of the acidic groups, was increased with the pH and showed a constant negative value at higher pH. Nevertheless, the amount of fixed charge on the RC membrane could be very small, as measured by Ramos et al. [33].

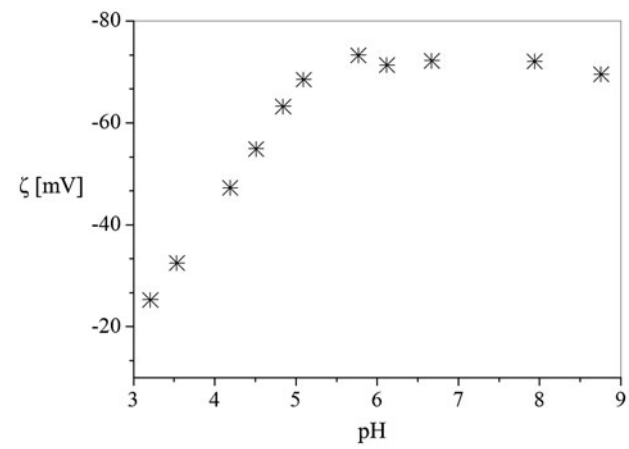

Fig. 3. Membrane zeta potential vs. pH.

3.2. The effect of electrocoagulation time on zeta potential and particle size in emulsions

In order to facilitate the following discussion, the reactions occurring at the electrodes are just briefly presented and discussed [23,34].

$$(-): 2H_2O + 2e^- \rightarrow H_{2(g)} + 2OH^-_{(aq)} \tag{8}$$

$$(+): 2H_2O \rightarrow O_{2(g)} + 4H^+_{(aq)} + 4e^- \tag{9}$$

$$(+): Al_{(s)} \rightarrow Al^{3+}_{(aq)} + 3e^- \tag{10}$$

The cathode produces hydrogen gas and hydroxyl ions (Eq. (8)) and the anode produces oxygen gas and aluminium ions (Eqs. (9) and (10)). Both hydrogen and oxygen gases are causing flotation and are able to partially remove some volatile pollutants from emulsions, if they exist [34,35]. During the time of EC, $Al^{3+}_{(aq)}$ hydrolyse forming di-charged, single charged and neutral aluminium hydroxide species, $Al(OH)^{2+}_{(aq)}$, $Al(OH)_2{}^+{}_{(aq)}$ and $Al(OH)_{3(s)}$, respectively. Other complexes also occur, but we assume our emulsion was in

its major proportion dominated by the aluminium species mentioned above [34]. The initial pH of the model emulsions was within the range 6.0–7.5 (Fig. 4), suggesting that the dominant species under our experimental conditions was $Al(OH)_{3(s)}$. At this pH range of model emulsions, other charged aluminium species also exist, yet in 10–100 times smaller concentrations, as explained by Holt et al. [34] and Harif et al. [23].

$Al(OH)_{3(s)}$ bridges the negative oil particles inducing coagulation and formation of irregular and porous flocs [22,23]. It stabilised the pH at 8, (Fig. 4) preventing the creation of $Al(OH)_4^-$ species that would restabilise emulsion [34]. The initial values of zeta potential (see Fig. 5(A)) of our emulsions corresponded to the measured initial pH, i.e. to the concentrations of the cutting-oils, −20 and −25 mV for the 0.1% for the 1%, respectively. The major part of emulsions represents polysiloxanes, which are known proton donors and are negatively charged in water solutions.

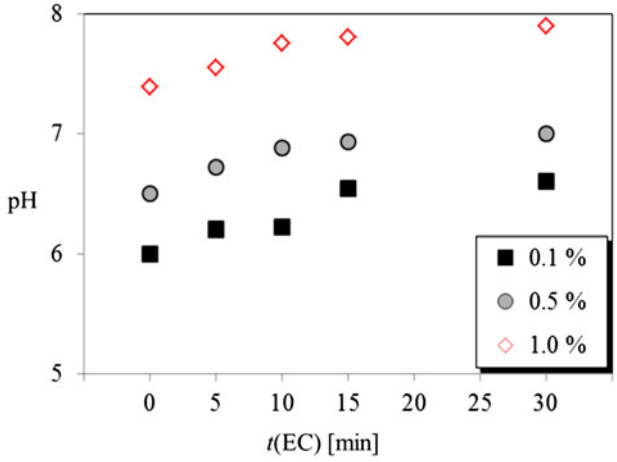

Fig. 4. Change in pH over the time of EC, for three different concentrations of model emulsions.

Fig. 5(A) shows the change of the zeta potential with the time of EC of three different cutting-oil emulsions. Current in our measurements was 0.2 A (100 A m^{-2}), therefore the concentration of Al which dissolved during the electrolysis, assuming 100% yield of current, may be calculated from Faraday's law and written as $C\ (Al^{3+})/mg\ L^{-1} = 1.86 \times 10^{-2}/mg\ L^{-1}\ s^{-1} \times t/s$. One can easily calculate that 33 mg of Al was necessary to completely destabilise 1 mg of cutting-oil in the 0.1% emulsion (destabilisation of 0.1% emulsion occurred after 30 min = 1,800 s). The zeta potential of the 0.1% model emulsion was significantly affected by the time of EC, i.e. the dissolved aluminium concentration. For instance, for a 0.1% emulsion only small concentration of the dissolved positively charged Al species was enough to neutralise the negative charge with substantial destabilisation occurring after only 15 min of EC. In the same manner, one may see that 330 mg of Al would have been necessary for the complete destabilisation of 1% emulsion (10 mg of oil) which would have been occurred after 285 min, which would have been obviously impractical and expensive. Because of long EC time of 1% emulsion, we focused to find the minimum time of EC that would significantly improve the MF performance.

Fig. 5(B) shows an increase in oil droplet/particle sizes with the EC time for all three concentrations of model cutting-oil emulsions. The particle growth trends of the cutting-oil suspensions were similar to recently reported kaolin suspensions' growth profiles, at a similar initial pHs [23]. Fortuitously, all emulsions showed a significant difference in charge neutralisation and particle growth trends with the time of EC. The charge was neutralised slowly, showing slow and

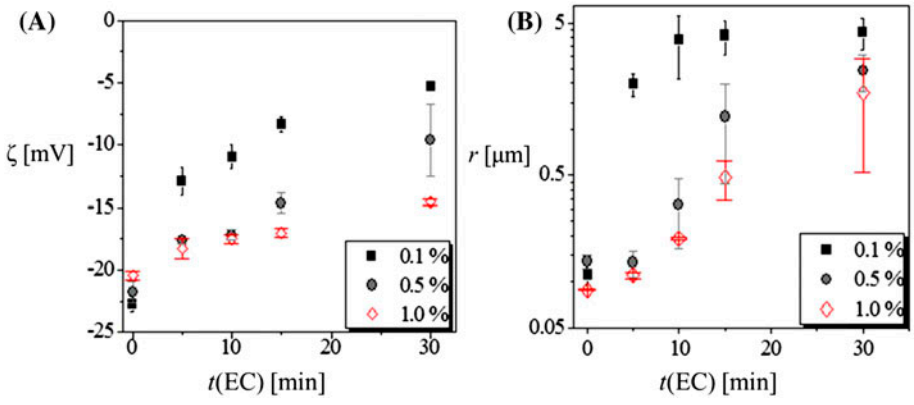

Fig. 5. The zeta potential and particle size measurements in dependence of the time of EC: (A) Change in the average zeta potential obtained from three independent measurements of model emulsions; (B) Increase in oil droplet/particle size as an average of three independent measurements.

monotonic growth and the particle growth was faster. This suggests that the particle growth is less dependent on the concentration of charged species and zeta potential of the emulsions and more dependent on the concentration of the precipitated $Al(OH)_{3(s)}$, which was the dominant species. It is likely that $Al(OH)_{3(s)}$ bridged the oil particles [18,23]; however, it had only slightly affected the overall zeta potential (charge) of the emulsions. Zeta potential was affected by positively charged aluminium species, particularly Al^{3+}, $Al(OH)^{2+}_{(aq)}$ and $Al(OH)_2{}^{+}{}_{(aq)}$, that exist in lower concentrations [34]. These lower concentrations of charged aluminium species were large enough to affect the charge of the 0.1% emulsions, nevertheless they just slightly affected the charge of 0.5 and 1.0% emulsions, as indicated in Fig. 5(A).

The most important observation from Fig. 4(B) is that larger particles started to form after only 10 min of EC, even for higher concentrations of the cutting-oil emulsions. Apparently, 10 min of EC (11 mg of Al) was sufficient enough to increase the average particle radii above the average pore radii of the MF membrane considered here. A slight increase in the average particle radii was sufficient to significantly improve MF performance, as will be shown below. The above presented data on the average particle and pore radii are used in the following sections to facilitate the interpretation of MF results.

3.3. Microfiltration of cutting-oil emulsions without and with EC pre-treatment

Fig. 6 summarises the flux decline data that had been measured and calculated using Eqs. (4)–(6). The concentration of cutting-oil in the emulsion had a significant effect on the permeate flux. Flux decline at $t = 0$ min represented MF without EC as a pre-treatment and it is briefly discussed before addressing the EC enhanced MF. At $t = 0$, the highest 1.0% model emulsion caused the highest total flux decline (FR), whereas the lowest 0.1% emulsion caused smaller, yet substantial flux decline FR ≈ 65%. The total flux decline in cross-flow MF is caused by two independent phenomena; concentration's polarisation, i.e. cake layer formation, and adsorption, i.e. pore clogging. In Fig. 6, the upper parts of the three columns designated for the time of EC present the flux decline caused by clogging, FR_{ADS}, and the lower parts of the columns represent flux decline caused by the concentration's polarisation, FR_{CP}.

FR_{CP} correlated with the concentration of oil. At the low concentrations of the oil (0.1%), FR_{CP} was about 13% and rose up to a maximum and constant of 35% for both higher concentrations of oil (0.5 and

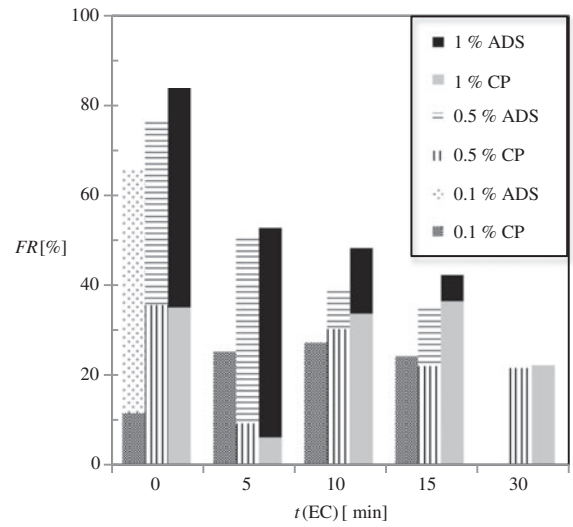

Fig. 6. MF flux decline, without EC pre-treatment ($t = 0$), and versus the time of EC pre-treatment.

1.0%). Fig. 6 apparently suggests that at higher concentrations of oil [10], 0.5 and 1.0% emulsions, respectively, a cake layer formed at the membrane's surface that increased the specific resistance to its maximum value and caused a constant maximum of FR_{CP} ≈ 35%. Flux decline caused by pore clogging, FR_{ADS}, was independent of the concentration of oil in the model emulsions and fairly constant at about 45%. The highest number of membrane pores (Fig. 2(B)) were larger or of similar size to the average colloidal particles (Fig. 5(B)) allowing the oil particles to enter the pores causing pore clogging [3,9]. This implies that a small concentration of the colloidal particles in water was sufficient enough to clog the membrane pores and cause irreversible fouling. FR_{ADS} obviously dominated the total flux decline in the MF of the cutting-oils and its contribution to FR was much larger than FR_{CP}, at any concentration of the model oil emulsions. When EC was used as a pre-treatment for MF feed, after only 10 min, a sharp decrease in FR_{ADS} may be noticed. Improved MF performance in terms of reduced FR_{ADS} was in fairly close agreement with the average pore and particle radii correlations with the time of EC, as presented in previous section.

For the 0.1% model, emulsion FR_{ADS} completely disappeared after only 5 min of EC whilst the remaining flux decline was caused solely by the concentration's polarisation i.e. cake layer. The reason for the complete disappearance of FR_{ADS} was obviously related to the rapid growth of the oil droplets during EC (Fig. 5(B)). Fig. 6 implies that FR_{ADS} could be completely eliminated even at higher concentrations of model cutting-oil emulsions by using 30 min of EC,

which is large improvement compared to 285 min that was expected to completely destabilise the emulsion.

Interestingly, 30 min of EC completely eliminated FR_{CP} for the lowest concentrations of oils whilst the FR_{CP} of 0.5 and 1.0% model emulsions was reduced significantly, almost by four times. Recently, Harif et al. [17,23] reported that flocs generated during the process of electrocoagulation are irregular in shape and porous. The EC constantly provided freshly formed aluminium hydroxides (see Section 3.2.) which generated highly porous and irregularly formed flocs, as measured by Harif et al. [23]. The oil particles aggregate with $Al(OH)_{3(s)}$ forming irregular floccules that form truly porous cake layers of high water permeability [5,13,23]. This explains the big decrease in total FR noticed in Fig. 6. EC enhanced MF—improved removal of oil.

Fig. 7 summarises the measured rejections at three different concentrations of model cutting-oil emulsions vs. the pre-treatment time. At $t = 0$, EC was not used as a pre-treatment and it could be noticed that the rejection of oil by the RC membranes increased with the concentration of cutting-oils, by up to 70% for the highest concentration used. Given that the membrane zeta potential was negative and constant at the corresponding working pH (Fig. 3) and the initial model emulsion zeta potentials were fairly similar (Fig. 5(A)), it may be deduced that the dominant mechanism during rejection was sieving, i.e. steric exclusion.

Previous sections showed that the average particle radii are similar to the average pore radii yet the measured rejection was lower than expected, especially at low concentrations of cutting-oils. Poor removal of oil could be as a major proportion attributed to the relatively large number of bigger pores (voids, Fig. 2(B)) which significantly contributed to the overall oil transport through the membrane.

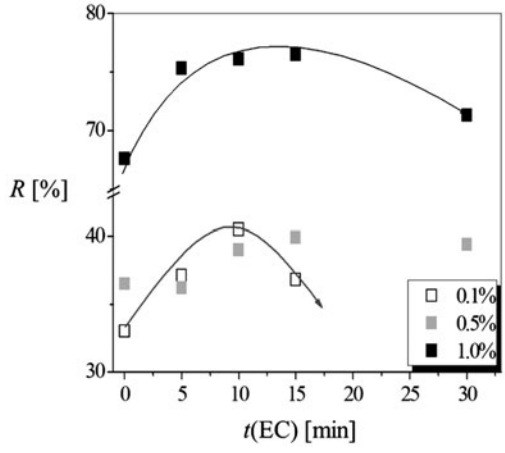

Fig. 7. MF removal of oil, R, depending on the time of EC used as a pre-treatment.

Using EC as a pre-treatment, the particles aggregated forming larger particles that enabled higher removal of oil and better permeate quality. At 0.1% of cutting-oil, the removal of oil increased by about 10% after only 10 min of EC, and then it dropped down to almost initial removal with further EC. It is well established that the stabilities of the floccules are highly affected by the shear stress which is herein imposed by the cross-flow velocity in the rectangular channel and spacer which covered MF membrane [5]. The stabilities of the floccules, formed by the mineral coagulants (aluminium or ferric ions) are, in general, lower than those bridged over polymeric coagulant [5]. This study did not check the stabilities and the sizes of the flocs under the shear stress within membrane unit. Nevertheless, some reasonable assumptions may explain the trends in Fig. 7. These assumptions are based on our experimental data and some previously reported work [5]. The UC030 membrane is bimodal, and whilst average particle radii are bigger than majority of pores, they are not bigger than the defects. The trend of the measured rejection in Fig. 7 suggests that only a small fraction of the oil particles become really large flocs, bigger than the membrane defects and thus retained this way increasing the overall removal of oil. Further increase in the floc size, related to the time of EC, probably resulted with the less stable flocs that destabilised under shear stress and broke into smaller flocs. Harif et. al. [23] indeed reported that $Al(OH)_{3(s)}$ forms very fragile flocs which could explain the sudden drop of rejection after 15 min of EC.

Increase in the sizes of the flocs was obviously beneficial for the reduction of clogging in smaller pores. In general, it may be deduced that the smaller pores poorly contributed to the transport of oil. This assumption was particularly valid for 0.1% model emulsions where 5 min of EC was enough to completely stop the pore clogging. The above-proposed explanation could realistically hold, as it explains the trends presented in Fig. 7 and it is in close agreement with previous studies [5,23].

4. Conclusions

The total flux decline in MF of cutting-oils was in major part dominated by the pore clogging that was independent on the cutting-oil concentration and significantly high. The shorter time of EC pre-treatment, 10 min, or only 11 mg of dissolved Al, was sufficient to significantly reduce pore clogging, even for higher concentrations of cutting-oil emulsions.

The EC pre-treatment induced the formation of highly permeable and porous cake layer on membrane surface. In the case of higher concentration model cutting-oils' emulsions, EC pre-treatment improved the cake layer water permeability by four times. The substantial improvement in the overall MF flux was in major part attributed to the continuous formation of $Al(OH)_{3(s)}$ as it formed cake layer made of porous and irregularly shaped flocs.

Acknowledgement

This work was supported by the Slovenian Research Agency (P2-0032), Ceepus Network program (CIII-SI-0708-01-1213-M-60450), and the Croatian Ministry of Science, Education and Sports through Project 125-1253008-3009 "Membrane and adsorption processes for removal of organic compounds in water treatment". The authors are grateful to Mr Werner Ruppricht representing MICRODYN-NADIR GmbH (Wiesbaden, Germany) for kindly supplying the microfiltration membrane used in this study.

List of symbols

ζ	—	zeta potential
R	—	rejection of oil by a microfiltration membrane
C_p	—	total carbon concentration in the permeate (mg dm^{-3})
C_f	—	total carbon concentration in the feed (mg dm^{-3})
FR	—	the total flux decline
FR_{ADS}	—	flux decline caused by adsorption and pore clogging
FR_{CP}	—	flux decline caused by concentration polarisation and cake layer formation
J_{wi}	—	initial virgin membrane flux measured with deionised water (m s^{-1})
J_s	—	flux measured with model cutting-oil emulsion (m s^{-1})
J_{wc}	—	flux that was measured with deionised water after the membrane had been flushed with deionised water (m s^{-1})
Φ	—	average swelling
$\Phi_{x,y\ or\ z}$	—	swelling in x, y or z direction
m_{wet}	—	mass of wet membrane sample (g)
m_{dry}	—	mass of dry membrane sample (g)
d_{wet}	—	height of wet membrane sample (mm)
d_{dry}	—	height of dry membrane sample (mm)
I	—	the current used in electrocoagulation (A)
t	—	time of the electrocoagulation (min)

References

[1] M. Gräfen, K. Hesse, D. Pollkläsner, W. Baumann, Generic scenario for the impact of cooling lubricants into the hydrosphere, Environ. Sci. Pollut. Res. 10 (2003) 301–307.
[2] P. Cañizares, F. Martínez, J. Lobato, M.A. Rodrigo, Break-up of oil-in-water emulsions by electrochemical techniques, J. Hazard. Mater. 145 (2007) 233–240.
[3] N. Hilal, G. Busca, F. Talens-Alesson, B.P. Atkin, Treatment of waste coolants by coagulation and membrane filtration, Chem. Eng. Process. 43 (2004) 811–821.
[4] J. Križan, A. Murić, I. Petrinic, M. Simonic, Recent developments in membrane treatment of spent cutting-oils: A review, Ind. Eng. Chem. Res. 52 (2013) 7603–7616.
[5] E. Barbot, S. Moustier, J.-Y. Bottero, P. Moulin, Coagulation and ultrafiltration: Understanding of the key parameters of the hybrid process, J. Membr. Sci. 325 (2008) 520–527.
[6] B. Chakrabarty, A.K. Ghoshal, M.K. Purkait, Ultrafiltration of stable oil-in-water emulsion by polysulfone membrane, J. Membr. Sci. 325 (2008) 427–437.
[7] N. Hilal, G. Busca, N. Hankins, A.W. Mohammad, The use of ultrafiltration and nanofiltration membranes in the treatment of metal-working fluids, Desalination 167 (2004) 227–238.
[8] H.J. Li, Y.M. Cao, J.J. Qin, X.M. Jie, T.H. Wang, J.H. Liu, Q. Yuan, Development and characterization of anti-fouling cellulose hollow fiber UF membranes for oil–water separation, J. Membr. Sci. 279 (2006) 328–335.
[9] A. Salahi, M. Abbasi, T. Mohammadi, Permeate flux decline during UF of oily wastewater: Experimental and modeling, Desalination 251 (2010) 153–160.
[10] G. van den Berg, I. Rácz, C. Smolders, Mass transfer coefficients in cross-flow ultrafiltration, J. Membr. Sci. 47 (1989) 25–51.
[11] V. Gekas, B. Hallström, Mass transfer in the membrane concentration polarization layer under turbulent cross flow: I. Critical literature review and adaptation of existing sherwood correlations to membrane operations, J. Membr. Sci. 30 (1987) 153–170.
[12] R.S. Faibish, Y. Cohen, Fouling and rejection behavior of ceramic and polymer-modified ceramic membranes for ultrafiltration of oil-in-water emulsions and microemulsions, Colloid. Surf. A 191 (2001) 27–40.
[13] T. Liu, Z.-L. Chen, W.-Z. Yu, J.-M. Shen, J. Gregory, Effect of two-stage coagulant addition on coagulation-ultrafiltration process for treatment of humic-rich water, Water Res. 45 (2011) 4260–4268.
[14] J. Zhong, X. Sun, C. Wang, Treatment of oily wastewater produced from refinery processes using flocculation and ceramic membrane filtration, Sep. Purif. Technol. 32 (2003) 93–98.
[15] G. Sharma, H.K. Shon, R. Aryal, S. Phuntsho, Performance evaluation of microfiltration with electrocoagulation and chemical coagulation pretreatment, Desalin. Water Treat. 34 (2011) 141–149.
[16] C. Guigui, J.C. Rouch, L. Durand-Bourlier, V. Bonnelye, P. Aptel, Impact of coagulation conditions

on the in-line coagulation/UF process for drinking water production, Desalination 147 (2002) 95–100.
[17] V. Lahoussine-Turcaud, M.R. Wiesner, J.-Y. Bottero, Fouling in tangential-flow ultrafiltration: The effect of colloid size and coagulation pretreatment, J. Membr. Sci. 52 (1990) 173–190.
[18] T. Harif, A. Adin, Characteristics of aggregates formed by electroflocculation of a colloidal suspension, Water Res. 41 (2007) 2951–2961.
[19] C.-L. Yang, Electrochemical coagulation for oily water demulsification, Sep. Purif. Technol. 54 (2007) 388–395.
[20] V.V. Keerthi, N. Balasubramanian, Electrocoagulation-integrated hybrid membrane processes for the treatment of tannery wastewater, Environ. Sci. Pollut. Res. 20 (2013) 7441–7449.
[21] D. Kumarasinghe, L. Pettigrew, L.D. Nghiem, Removal of heavy metals from mining impacted water by an electrocoagulation-ultrafiltration hybrid process, Desalin. Water Treat. 11 (2009) 66–72.
[22] O. Sahu, B. Mazumdar, P.K. Chaudhari, Treatment of wastewater by electrocoagulation: A review, Environ. Sci. Pollut. Res. 21 (2014) 2397–2413.
[23] T. Harif, M. Khai, A. Adin, Electrocoagulation versus chemical coagulation: Coagulation/flocculation mechanisms and resulting floc characteristics, Water Res. 46 (2012) 3177–3188.
[24] P. Cañizares, F. Martínez, C. Jiménez, C. Sáez, M.A. Rodrigo, Coagulation and electrocoagulation of oil-in-water emulsions, J. Hazard. Mater. 151 (2008) 44–51.
[25] A.K. Yadav, L. Singh, A. Mohanty, S. Satya, T.R. Sreekrishnan, Removal of various pollutants from wastewater by electrocoagulation using iron and aluminium electrode, Desalin. Water Treat. 46 (2012) 352–358.
[26] P.K. Holt, Electrocoagulation: Unravelling and synthesising the mechanisms behind a water treatment process, Doctoral thesis, Faculty of Engineering, The University of Sydney, 2006.
[27] Y.-Q. Wang, T. Wang, Y.-L. Su, F.-B. Peng, H. Wu, Z.-Y. Jiang, Remarkable reduction of irreversible fouling and improvement of the permeation properties of poly(ether sulfone) ultrafiltration membranes by blending with pluronic F127, Langmuir 21 (2005) 11856–11862.
[28] K.M. Persson, V. Gekas, G. Trägårdh, On the presence of double log-normal permeability distributions in ultrafiltration membranes, J. Membr. Sci. 93 (1994) 105–113.
[29] S. Bason, Y. Kaufman, V. Freger, Analysis of ion transport in nanofiltration using phenomenological coefficients and structural characteristics, J. Phys. Chem. B 114 (2010) 3510–3517.
[30] S. Torquato, Random Heterogeneous Materials: Microstructure and Macroscopic Properties, Springer, New York, NY, 2002.
[31] M. Al Manasrah, M. Kallioinen, H. Ilvesniemi, M. Mänttäri, Recovery of galactoglucomannan from wood hydrolysate using regenerated cellulose ultrafiltration membranes, Bioresour. Technol. 114 (2012) 375–381.
[32] J. Wagner, Membrane Filtration Handbook: Practical Tips and Hints, Osmonics, Cambrige, 2001.
[33] J. Ramos, C. Milano, V. Romero, S. Escalera, M. Alba, M. Vázquez, J. Benavente, Water effect on physical–chemical and elastic parameters for a dense cellulose regenerated membrane: Transport of different aqueous electrolyte solutions, J. Membr. Sci. 352 (2010) 153–159.
[34] P.K. Holt, G.W. Barton, C.A. Mitchell, The future for electrocoagulation as a localised water treatment technology, Chemosphere 59 (2005) 355–367.
[35] E. Ofin, Y. Oren, A. Adin, Electroflocculation: The effect of zeta-potential on particle size, Desalination 204 (2007) 33–38.